NCTS-ECP/1501

Electronic and nuclear contributions in sub-GeV dark matter scattering: A case study with hydrogen

Jiunn-Wei Chen,[1,2,3] Hsin-Chang Chi,[4] C.-P. Liu,[4] Chih-Liang Wu,[1] and Chih-Pan Wu[1]

[1] *Department of Physics, National Taiwan University, Taipei 10617, Taiwan*

[2] *Center for Theoretical Sciences and Leung Center for Cosmology and Particle Astrophysics, National Taiwan University, Taipei 10617, Taiwan*

[3] *Helmholtz-Institut für Strahlen- und Kernphysik and Bethe Center for Theoretical Physics, Universität Bonn, D-53115 Bonn, Germany*

[4] *Department of Physics, National Dong Hwa University, Shoufeng, Hualien 97401, Taiwan*

Abstract

Scattering of sub-GeV dark matter (DM) particles with hydrogen atoms is studied in this paper. The interactions of DM with electrons and nucleons are both included and formulated in a general framework based on nonrelativistic effective field theory. On the assumption of same dark matter coupling strengths, it is found that DM–electron interactions dominate the inelastic atomic transitions to discrete excited states and ionization continuum around the threshold regions, and DM–nucleon interactions become more important with increasing energy and dominate in elastic scattering. The conclusion should apply, qualitatively, to practical detector species so that electronic and nuclear contributions in DM scattering processes can be disentangled, while issues including binding effects and recoil mechanism in many-body systems call for more detailed calculations.

I. INTRODUCTION

The existence of dark matter (DM) has been concretely established based on gravitational evidences from various scales of the universe. However, its composition and non-gravitational interactions, if any, are still unknown. Among all DM candidates, the weakly-interacting massive particles (WIMPs) receive most attention mainly because of the so-called "WIMP miracle": with DM particle mass $m_\chi \sim 10\,\mathrm{GeV}$–$1\,\mathrm{TeV}$ and self-annihilation cross section similar to the one of the weak interaction, WIMPs can explain the relic DM abundance of the universe. By looking for nuclear recoil triggered by WIMP scattering in detectors, null results of direct searches have ruled out quite some WIMP parameter space (for current status, see, e.g., [1] and references therein), and future multi-ton experiments will further improve the limit (or make discovery).

On the other hand, the dark sector consisting of light DM (LDM) particles with masses below 10 GeV also attracts interests recently (for overview, see, e.g., [2] and references therein). First of all, there is no reason to exclude such possibilities a priori, and in fact, many well-motivated models predict their existence: for example, WIMPless [3, 4] and asymmetric DM with m_χ varying between MeV to GeV scales, several proposals at MeV ranges [5–10], and keV ranges including bosonic super-WIMP [11], axinos [12–14], and sterile neutrinos [15–19]. Furthermore, in order to accommodate low-energy anomalies in astrophysical sources such as the 511 keV [20, 21] (reviewed in [22]) and 3.5 keV [23, 24] emission lines, and the GeV γ-ray excesses in the Galactic Center [25, 26], LDM are often proposed as possible answers.

As most of these LDM candidates can not produce observable nuclear recoils in present-day (and near-future) detectors, direct searches for them have to rely on electron recoils. Not like WIMP searches, they are used to constrain DM–electron interactions [27, 28]. Alternative searches through indirect signals and colliders are also reported [29–31].

DM–electron interactions are interesting from another aspect beyond LDM: To reconcile the tension between the light WIMP signal ($m_\chi \sim 10\,\mathrm{GeV}$) reported by the DAMA/LIBRA experiment [32–34] and stringent constraints set by other direct experiments on WIMP–nucleon interactions, models of DM being lepto-philic but not hadro-philic provide viable solutions (see, e.g., [35–37]). At even higher masses, the annihilation of WIMPs are among the favored explanations of the positron excesses observed by PAMELA [38, 39], Fermi-

LAT [40], and AMS-02 [41, 42] experiments.

If DM interacts both with electrons and nucleons, an important question naturally arises: In a specific DM scattering process which a direct search detector is build to look for, what are the contributions from the electronic and nuclear degrees of freedom? Even though the current common practice in constraining DM interactions is one-type-at-a-time, it is necessary to keep in mind that events measured by a detector are a sum from all possible sources. Furthermore, it is desirable from the experimental point of view to determine which process and kinematic region would be best to constrain a certain type of DM interactions with electrons or nucleons. For this purpose, one has to rely on theoretical analysis.

In this article, we attempt to address the above questions using the simplest atom: hydrogen – where most calculations can be carried out analytically – and study its scattering with nonrelativistic LDM particles of a MeV–GeV mass range. As the associated energy and momentum transfer of such scattering processes overlap with typical atomic scales, one expects that atomic physics plays an important role and issues like binding effects and electron/nuclear recoils require detailed study. The simplistic setup of hydrogen should therefore provide useful qualitative understanding which applies to more intricate systems.

The paper is organized as follows. In Section II, the general formalism is developed for scattering channels including elastic, discrete excitation, and ionization. The DM–electron and DM–nucleon interactions are formulated in a general way based on effective field theory (EFT). In addition to commonly-discussed spin-independent and spin-dependent contact interactions, which are the leading-order terms in the EFT expansion, we also include the possibility of long-ranged DM interactions (for example, through kinetic mixing of dark and normal photons) and a few next-to-leading-order terms. In Section II, we present and discuss our results, and infer from these generic features that will apply to other atoms including those practically being used in mainstream DM detectors. Finally, a summary is given in Section IV.

II. FORMALISM

Direct searches of DM look for signals as results of DM scattering off normal matter. As the nature of DM and its non-gravitational interactions with normal matter are still unknown, instead of considering specific, well-motivated models, we adopt a general approach

based on effective field theory (EFT). A nonrelativistic (NR) EFT that accommodates scalar, fermionic, and vector DM particles with velocity $v_\chi \ll 1$ [1] and their interactions with protons (p) and neutrons (n) via intermediate scalar and vector bosons is formulated in Ref. [43], and fully worked out to next-to-next-to-leading order in Ref. [44]. In this work, we further take electrons into account, and focus on the kinematic region where electrons also behave like NR particles.

At leading order (LO), the effective interaction takes the form

$$\mathcal{L}_{\rm int}^{\rm (LO)} = \sum_{f=e,p,n} \Big\{ c_1^{(f)} (\chi^\dagger \chi)(f^\dagger f) + c_4^{(f)} (\chi^\dagger \vec{S}_\chi \chi) \cdot (f^\dagger \vec{S}_f f) + d_1^{(f)} \frac{1}{q^2} (\chi^\dagger \chi)(f^\dagger f) + d_4^{(f)} \frac{1}{q^2} (\chi^\dagger \vec{S}_\chi \chi) \cdot (f^\dagger \vec{S}_f f) \Big\} \,, \tag{1}$$

where χ and f denote the NR DM and fermion fields, respectively; $\vec{S}_{\chi,f}$ are their spin operators (scalar DM particles have null $\vec{S}_\chi$); the magnitude of the DM 3-momentum transfer $q = |\vec{q}|$ depends on the DM energy transfer T and its scattering angle θ. Note that we use the same nomenclature as in [44] for the low-energy constants (LECs) $c_i^{(f)}$'s that characterize the types of the χ–f contact interactions. Correspondingly the LECs $d_i^{(f)}$'s are used to describe potential $U(1)$-like, long-ranged χ–f interactions that are results of, e.g., mixing of dark and ordinary photons via $\epsilon F'_{\mu\nu} F^{\mu\nu}$ where the $F'_{\mu\nu}$ and $F_{\mu\nu}$ refer to the field tensors of dark and ordinary photon, respectively, and ϵ the mixing angle. These LECs corresponds to the ones of [43] by $c_1 \to h_1$, $c_4 \to h_2$, $d_1 \to l_1$, and $d_4 \to l_2$.

To simplify the presentation of the full scattering formula for an unpolarized DM scattering off a hydrogen atom, we start with the simplified case where only one of the LECs is assumed to be nonzero. (Note. This is the conventional practice in DM searches). Following the standard scattering theory (for more details, see, e.g., Ref. [45]), the differential cross section in the laboratory frame for DM being scattered by the $c_1^{(e)}$ term alone in Eq. (1) into the final 3-momentum $\vec{k}_2$ with an infinitesimal phase volume d^3k_2 is expressed by

$$d\sigma|_{c_1^{(e)}} = \frac{2\pi}{v_\chi} \sum_F \overline{\sum_I} |\, \langle F | c_1^{(e)} e^{i \frac{\mu}{m_e} \vec{q}\cdot\vec{r}} | I \rangle \,|^2 \delta(T - E_{\rm CM} - (E_F - E_I)) \frac{d^3k_2}{(2\pi)^3} \,. \tag{2}$$

[1] We adopt the natural units $c = 1$ and $\hbar = 1$.

The reduced mass $\mu = m_e m_p/(m_e + m_p)$ with $m_{e(p)}$ being the mass of electron (proton); for later use, the mass of hydrogen is designated $M_{\rm H} = M - B$ with $M = m_e + m_p$ and B the binding energy. The initial state $|I\rangle$ denotes the hydrogen atom at the ground state, i.e., the spatial part $|I\rangle_{\rm spatial} = |1s\rangle$. The Dirac delta function imposes the energy conservation that the energy deposited by DM equals to the recoil energy of the atomic center of mass, $E_{\rm CM}$, plus the internal excitation energy $E_F - E_I$ of the atom.

Depending on the nature of the final state $\langle F|$, the scattering processes are classified as

1. elastic scattering (el): ${}_{\rm spatial}\langle F| = \langle 1s|$; $E_{\rm CM} = q^2/(2M_{\rm H})$ and $E_F - E_I = 0$,

2. discrete excitation (ex), ${}_{\rm spatial}\langle F| = \langle nlm_l|$ with $(n, l, m_l) \neq (1, 0, 0)$; $E_{\rm CM} = q^2/(2M_{\rm H})$ and $E_F - E_I = E_{nl} - E_{1s}$,

3. ionization (ion): ${}_{\rm spatial}\langle F| = \langle \vec{p}_r|$ with $\vec{p}_r$ denoting the relative momentum in the CM frame; $E_{\rm CM} = q^2/(2M)$ and $E_F - E_I = B + p_r^2/(2\mu)$.

The symbol $\overline{\sum}_I$ means an average over the initial magnetic (and spin, when spin operators are involved) states; $\sum_F$ means a sum over all the final magnetic and spin (also spin, too) states for elastic scattering and discrete excitation, while for ionization, the sum over magnetic states is replaced by $\int d^3\vec{p}_r/(2\pi)^3$.

The analytic forms of discrete and continuum hydrogenic wave functions:

$$\langle 100|\vec{r}\rangle = \frac{1}{\sqrt{\pi}} Z^{\frac{3}{2}} e^{-Z\bar{r}}\,, \tag{3}$$

$$\langle nlm_l|\vec{r}\rangle = \frac{1}{(2l+1)!}\sqrt{\frac{(n+l)!}{2n(n-l-1)!}}\left(\frac{2Z}{n}\right)^{\frac{3}{2}} e^{-\frac{Z\bar{r}}{n}}\left(\frac{2Z\bar{r}}{n}\right)^{l} {}_1F_1\left(-(n-l-1), 2l+2, \frac{2Z\bar{r}}{n}\right) \times Y_l^{m_l *}(\theta,\phi)\,, \tag{4}$$

$$\langle \vec{p}_r|\vec{r}\rangle = e^{\frac{\pi Z}{2\bar{p}_r}}\Gamma\left(1 - \frac{iZ}{\bar{p}_r}\right) e^{-i\vec{p}_r\cdot\vec{r}}\, {}_1F_1\left(\frac{iZ}{\bar{p}_r}, 1, i(p_r r + \vec{p}_r\cdot\vec{r})\right)\,, \tag{5}$$

are given in atomic units [so that barred quantities $\bar{r} = r m_e\alpha$ and $\bar{p}_r = p_r/(m_e\alpha)$], where $\Gamma(z)$ and ${}_1F_1(a, b, z)$ are the Gamma and confluent hypergeometric functions, respectively. By the Nordsieck integration techniques [46–49], we can calculate matrix elements of the transition operator $e^{i\vec{\kappa}\cdot\vec{r}}$, where $\vec{\kappa}$ denotes the three momentum transfer, analytically. The

response function relevant for transitions to discrete states is found to be

$$
\begin{aligned}
R^{(nl)}(\kappa) &= \sum_{m_l} |\, \langle nlm_l | e^{i\vec{\kappa}\cdot\vec{r}} | 1s \rangle \,|^2 \\
&= (2l+1)\mathcal{I}^2_{nl}\,, \qquad (6) \\
\mathcal{I}_{nl}(\kappa) &= \frac{(-1)^{n-l-1}}{4n^2(2l+1)!}\sqrt{\frac{\pi(n+l)!}{(n-l-1)!}}\frac{\Gamma(2l+2)}{\Gamma(n+l+1)}\frac{\Gamma(2l+3)}{\Gamma(l+3/2)}(\frac{\bar{\kappa}}{4Z})^l \\
&\times \left(\frac{d}{dt}\right)^{n-l-1}\left[(1-t)^{n+l+1}\left((1-t)^2+(\frac{\bar{\kappa}}{2Z})^2\right)^{-l-2}\right]\Bigg|_{t=0}\,, \qquad (7)
\end{aligned}
$$

which is dimensionless. The response function relevant for transitions to continuum is

$$
\begin{aligned}
R^{(ion)}(\kappa) &= \int d^3p_r |\, \langle \vec{p}_r | e^{i\vec{\kappa}\cdot\vec{r}} | 1s \rangle \,|^2 \delta(T - B - \frac{\vec{q}^2}{2M} - \frac{\vec{p}_r^2}{2\mu}) \\
&= \left.\frac{2^8 Z^6 \bar{q}^2 (3\bar{\kappa}^2 + \bar{p}_r^2 + Z^2)\exp\left[-\frac{2Z}{\bar{p}_r}\tan^{-1}\left(\frac{2Z\bar{p}_r}{\bar{\kappa}^2 - \bar{p}_r^2 + Z^2}\right)\right]}{3m_e\alpha^2((\bar{\kappa}+\bar{p}_r)^2+Z^2)^3((\bar{\kappa}-\bar{p}_r)^2+Z^2)^3(1-\exp^{\frac{-2\pi Z}{\bar{p}_r}})}\right|_{p_r=\sqrt{2\mu\left(T-B-\frac{\vec{q}^2}{2M}\right)}}\,, \\
& \qquad (8)
\end{aligned}
$$

where the factor of $m_e\alpha^2$ in the denominator gives the dimension as the energy conserving delta function is included in the definition.

Using the generic response functions obtained above, the single differential cross section with respect to energy transfer, $d\sigma/dT$, can be compactly expressed. For elastic scattering or discrete excitation to the final discrete level (nl)

$$
\left.\frac{d\sigma^{(nl)}}{dT}\right|_{c_1^{(e)}} = \frac{1}{2\pi}\frac{m_{\rm H}}{v_\chi^2}\left|c_1^{(e)}\right|^2 R^{(nl)}(\kappa = \frac{\mu}{m_e}q)\,, \qquad (9)
$$

$$
\text{with} \quad q^2 = 2M_{\rm H}(T - (E_{nl} - E_{1s}))\,. \qquad (10)
$$

The $1/v_\chi^2$ factor in Eq. (9) comes from two sources with each one contributing $1/v_\chi$: (i) division by flux in $d\sigma/dT$ and (ii) the integration of DM scattering angle $\cos\theta$ with respect to the energy conserving delta function. Note that it does not lead to physical sigularity when taking an extremely NR limit $v_\chi \to 0$, since the DM flux and kinetic energy both approach zero. The magnitude of q is determined by energy conservation, or equivalently, the scattering angle $\cos\theta$ is fixed once the energy transfer T for such 2-to-2-body scattering is known. For ionization processes:

$$\left.\frac{d\sigma^{(ion)}}{dT}\right|_{c_1^{(e)}} = \frac{1}{2\pi}\frac{m_\chi}{v_\chi}k_2\int d\cos\theta\,\left|c_1^{(e)}\right|^2 R^{(ion)}(\kappa=\frac{\mu}{m_e}q), \tag{11}$$

$$\text{with}\quad \min\left\{1,\max\left[-1,\frac{k_1^2+k_2^2-2M(T-B)}{2k_1k_2}\right]\right\}\leq\cos\theta\leq 1\,, \tag{12}$$

where $k_1 = m_\chi v_\chi$ and $k_2 = (m_\chi^2 v_\chi^2 - 2m_\chi T)^{1/2}$ are the magnitudes of the initial and final momentum, respectively. Because the final atomic state has two bodies to share the transferred energy and momentum, the DM scattering angle $\cos\theta$ now can span a finite range for a given energy transfer T.

Next we consider the $d_1^{(e)}$ term. Because its Lagrangian differs from $c_1^{(e)}$ term only by a kinematic factor $1/q^2$ (which only cause a rescaling of transition matrix elements), it can easily be calculated by replacing $c_1^{(e)}$ to $d_1^{(e)}/q^2$ in both Eqs. (9) and (11). If both terms exist, then one has to take their coherent interference into account, so that the coupling in front of the response functions becomes $c_1^{(e)} + d_1^{(e)}/q^2$.

Unlike the $c_1^{(e)}$ and $d_1^{(e)}$ terms, which are independent of the spins of the DM and the scattered particles, the $c_4^{(e)}$ and $d_4^{(e)}$ terms give rise to what typically called spin-dependent interactions. Their matrix elements for unpolarized scattering involve additionally initial spin average and final spin sum. For a spinor with spin quantum number s and m_s, it yields

$$\sum_{m_s'}\overline{\sum_{m_s}}\langle s,m_s'|S_a|s,m_s\rangle\,\langle s,m_s'|S_b|s,m_s\rangle^* = \frac{1}{3}s(s+1)\delta_{ab}\,. \tag{13}$$

With the DM spin s_χ and the electron spin $s_e = 1/2$, the spin averages and sums applied to both the DM and electron parts yield a product: $s_\chi(s_\chi+1)/4$. Other than this factor, the rest of spatial matrix elements are completely the same as in the $c_1^{(e)}$ and $d_1^{(e)}$ case. As a result, the corresponding scattering formula can be obtained by changing $\left|c_1^{(e)} + d_1^{(e)}/q^2\right|^2$ to $\frac{1}{4}s_\chi(s_\chi+1)\left|c_4^{(e)} + d_4^{(e)}/q^2\right|^2$ in both Eqs. (9) and (11).

It is worthwhile to point out here that there is no interference between the spin-independent interactions with c_1, d_1 and the spin-dependent one with c_4, d_4, in unpolarized scattering, since the trace of a spin matrix is zero.

Now we consider the cases when DM scatters off the proton instead of the electron. Besides the trivial change of LECs, the most important difference is due to the fact that the proton is much closer to the atomic center of mass than the electron. After factoring out the

center-of-mass motion, the resulting atomic transition operators in its intrinsic frame are

$$\rho^{(e)}(\vec{q}) = e^{i\frac{\mu}{m_e}\vec{q}\cdot\vec{r}}\,, \tag{14}$$

$$\rho^{(p)}(\vec{q}) = e^{-i\frac{\mu}{m_p}\vec{q}\cdot\vec{r}}\,, \tag{15}$$

for the electron and the proton, respectively. This leads to the following change of the corresponding response functions:

$$R_e^{(nl,ion)} = R^{(nl,ion)}(\kappa = \frac{\mu}{m_e}q)\,, \tag{16}$$

$$R_p^{(nl,ion)} = R^{(nl,ion)}(\kappa = \frac{\mu}{m_p}q)\,, \tag{17}$$

and similarly in the differential cross section formulae, Eqs. (9) and (11).

Finally we can summarize the above derivation and obtain the differential cross section formulae for DM scattering off the hydrogen atom at LO. For transitions to discrete states:

$$\begin{aligned}\left.\frac{d\sigma^{(nl)}}{dT}\right|_{\rm LO} = \frac{1}{2\pi}\frac{m_{\rm H}}{v_\chi^2}\Bigg\{\sum_{f=e,p}\left(\left|c_1^{(f)}+\frac{d_1^{(f)}}{q^2}\right|^2+\frac{1}{4}s_\chi(s_\chi+1)\left|c_4^{(f)}+\frac{d_4^{(f)}}{q^2}\right|^2\right)R_f^{(nl)}\\ +2\left(c_1^{(e)}+d_1^{(e)}/q^2\right)\left(c_1^{(p)}+d_1^{(p)}/q^2\right)^* R_{ep}^{(nl)}\Bigg\}\Bigg|_{q^2=2M_{\rm H}(T-(E_{nl}-E_{1s}))}\,,\end{aligned} \tag{18}$$

and for ionizations:

$$\begin{aligned}\left.\frac{d\sigma^{(ion)}}{dT}\right|_{\rm LO} = \frac{1}{2\pi}\frac{m_\chi}{v_\chi}k_2\int d\cos\theta\Bigg\{\sum_{f=e,p}\left(\left|c_1^{(f)}+\frac{d_1^{(f)}}{q^2}\right|^2+\frac{1}{4}s_\chi(s_\chi+1)\left|c_4^{(f)}+\frac{d_4^{(f)}}{q^2}\right|^2\right)R_f^{(ion)}\\ +2\left(c_1^{(e)}+d_1^{(e)}/q^2\right)\left(c_1^{(p)}+d_1^{(p)}/q^2\right)^* R_{ep}^{(ion)}\Bigg\}\Bigg|_{p_r^2=2\mu(T-B-q^2/(2M))}\,.\end{aligned} \tag{19}$$

In these formulae, there are two new response functions $R_{ep}^{(nl,ion)}$ defined, which describe the nontrivial interference between the spin-independent χ–e and χ–p amplitude; they are

$$R_{ep}^{(nl)} = \sqrt{R_e^{(nl)}R_p^{(nl)}}\,, \tag{20}$$

and

$$R_{ep}^{(ion)} = \int d^3p_r\,\langle\vec{p}_r|e^{i\frac{\mu}{m_e}\vec{q}\cdot\vec{r}}|1s\rangle\,\langle\vec{p}_r|e^{-i\frac{\mu}{m_p}\vec{q}\cdot\vec{r}}|1s\rangle^*\,\delta(T-B-\frac{\vec{q}^2}{2M}-\frac{\vec{p}_r^2}{2\mu})\,. \tag{21}$$

Note that there is no interference between the $c_4^{(e)}$ and $c_4^{(p)}$ terms, nor between the $d_4^{(e)}$ and $d_4^{(p)}$ terms, as they involve different spin operators with each of them traceless.

Even though we mainly concentrate on the LO interaction with DM in this article, we shall also consider a few terms at next-to-leading order (NLO):

$$\mathcal{L}_{\rm int}^{\rm (NLO)} = \sum_{f=e,p,n} \Big\{ c_{10}^{(f)} (\chi^\dagger \chi)(f^\dagger i\vec{\sigma}_f \cdot \vec{q} f) + c_{11}^{(f)} (\chi^\dagger i\vec{\sigma}_\chi \cdot \vec{q}\chi)(f^\dagger f) + d_{10}^{(f)} \frac{1}{q^2} (\chi^\dagger \chi)(f^\dagger i\vec{\sigma}_f \cdot \vec{q} f) + d_{11}^{(f)} \frac{1}{q^2} (\chi^\dagger i\vec{\sigma}_\chi \cdot \vec{q}\chi)(f^\dagger f) \Big\} + \cdots \tag{22}$$

They translate into the ones of [43] by $c_{11} \to h_1^{'}$, $c_{10} \to h_2^{'}$, $d_{11} \to l_1^{'}$, and $d_{10} \to l_2^{'}$. Because the spin operators that come with the $c_{11}^{(e,p)}$ and $c_{10}^{(e,p)}$ terms are mutually independent (after spin average and sum) with each other except for the interference between $c_{11}^{(e)}$ and $c_{11}^{(p)}$, and also with all LO terms, including them into Eqs. (18) and (19) is straightforward by

$$\begin{aligned}
&\left(\left| c_1^{(f)} + \frac{d_1^{(f)}}{q^2} \right|^2 + \frac{1}{4} s_\chi (s_\chi + 1) \left| c_4^{(f)} + \frac{d_4^{(f)}}{q^2} \right|^2 \right) \\
&\to \left(\left| c_1^{(f)} + \frac{d_1^{(f)}}{q^2} \right|^2 + \frac{1}{4} s_\chi (s_\chi + 1) \left| c_4^{(f)} + \frac{d_4^{(f)}}{q^2} \right|^2 + \frac{1}{3} s_\chi (s_\chi + 1) q^2 \left| c_{11}^{(f)} + \frac{d_{11}^{(f)}}{q^2} \right|^2 + \frac{1}{4} q^2 \left| c_{10}^{(f)} + \frac{d_{10}^{(f)}}{q^2} \right|^2 \right) \\
&\left(c_1^{(e)} + d_1^{(e)}/q^2 \right) \left(c_1^{(p)} + d_1^{(p)}/q^2 \right)^* \\
&\to \left(c_1^{(e)} + d_1^{(e)}/q^2 \right) \left(c_1^{(p)} + d_1^{(p)}/q^2 \right)^* + \frac{1}{3} s_\chi (s_\chi + 1) q^2 \left(c_{11}^{(e)} + d_{11}^{(e)}/q^2 \right) \left(c_{11}^{(p)} + d_{11}^{(p)}/q^2 \right)^* ,
\end{aligned} \tag{23}$$

where similar argument is applied to the $d_{11}^{(e,p)}$ and $d_{10}^{(e,p)}$ terms.

III. RESULTS AND DISCUSSIONS

In this section, we give numerical results for two different DM masses: (i) $m_\chi = 1\,\mathrm{GeV}$ and (ii) $m_\chi = 50\,\mathrm{MeV}$, and with a nonrelativistic velocity $v_\chi = 10^{-3}$. Our main purpose is to illustrate and discuss how electron and proton respectively contribute to the scattering processes for specified EFT interaction terms and reaction channels. For clarity in presentation, we ignore all interference terms and assume the DM interaction strengths with electron and

proton are the same when making comparisons between the electronic and nuclear contributions. It should be borne in mind that the total cross section is a sum of all contributions from electron and proton with interference terms included.

A. LO Interactions of c_1, d_1, c_4, and d_4

The upper two panels of Fig. 1 show the differential cross sections $d\sigma/dT$ for DM scattering with $m_\chi = 1\,\text{GeV}$ and the c_1-type interactions. For the nuclear part (right panel), the elastic scattering dominates all other channels by orders of magnitude. The reason is obvious: Since the momentum scale that determines the nuclear response $\kappa_p = \mu/m_p q \sim \mu/m_p m_\chi v_\chi \sim 0.5\,\text{keV}$ is smaller than the inverse of atomic size, $m_e\alpha \sim 3\,\text{keV}$, it is a good approximation that the nuclear charge operator can be expanded as $\rho(\vec{\kappa}_p) \sim 1 - i\vec{\kappa}_p \cdot \vec{r} + \ldots$ Unlike the elastic scattering, all inelastic channels have no leading-order contributions because of wave function orthogonality. Also because the next-leading-order operator is a dipole operator, the excitations to final p-orbitals or continuum are more probable than other discrete states. For the electronic part (left panel), the results change dramatically. First, as the momentum scale that determines the electronic response $\kappa_e = \mu/m_e q \sim \mu/m_e m_\chi v_\chi \sim 1\,\text{MeV}$ is much bigger than the inverse of atomic size, the electric charge operator $\rho(\vec{\kappa}_e) = e^{i\vec{\kappa}_e\cdot\vec{r}}$ becomes highly oscillating. As a result, the elastic differential cross section shows the familiar form factor suppression. On the other hand, in discrete excitations, one does observe much larger cross sections in near-threshold regions. The reason is most of the energy transferred T by DM is given to internal excitation; this leaves the 3-momentum transfer $q = \sqrt{2M_\text{H}(T - (E_{nl} - E_{1s}))}$ becoming quite small so that the form factor suppression is less severe. Among all reaction channels arising from the $c_1^{(e)}$-type interaction, the ionization channel is the dominant one in most of the kinematic region, for it can access more of the kinematic phase space with small q. In addition, the peaks near discrete excitation thresholds also provide good observation windows for not only the large cross section but also the clean signal of deexcitation photons of definite energies.

In the lower two panels of Fig. 1, the results for the d_1-type interactions are shown. The numerical changes from the previous c_1-type results are mainly due to adding $1/q^2$ factor in the scattering amplitude (or $1/q^4$ in the double differential cross section). Because $q^2 = 2m_\text{H}T$ in elastic scattering, this leads to an extra $1/T^2$ dependence in $d\sigma/dT$ and

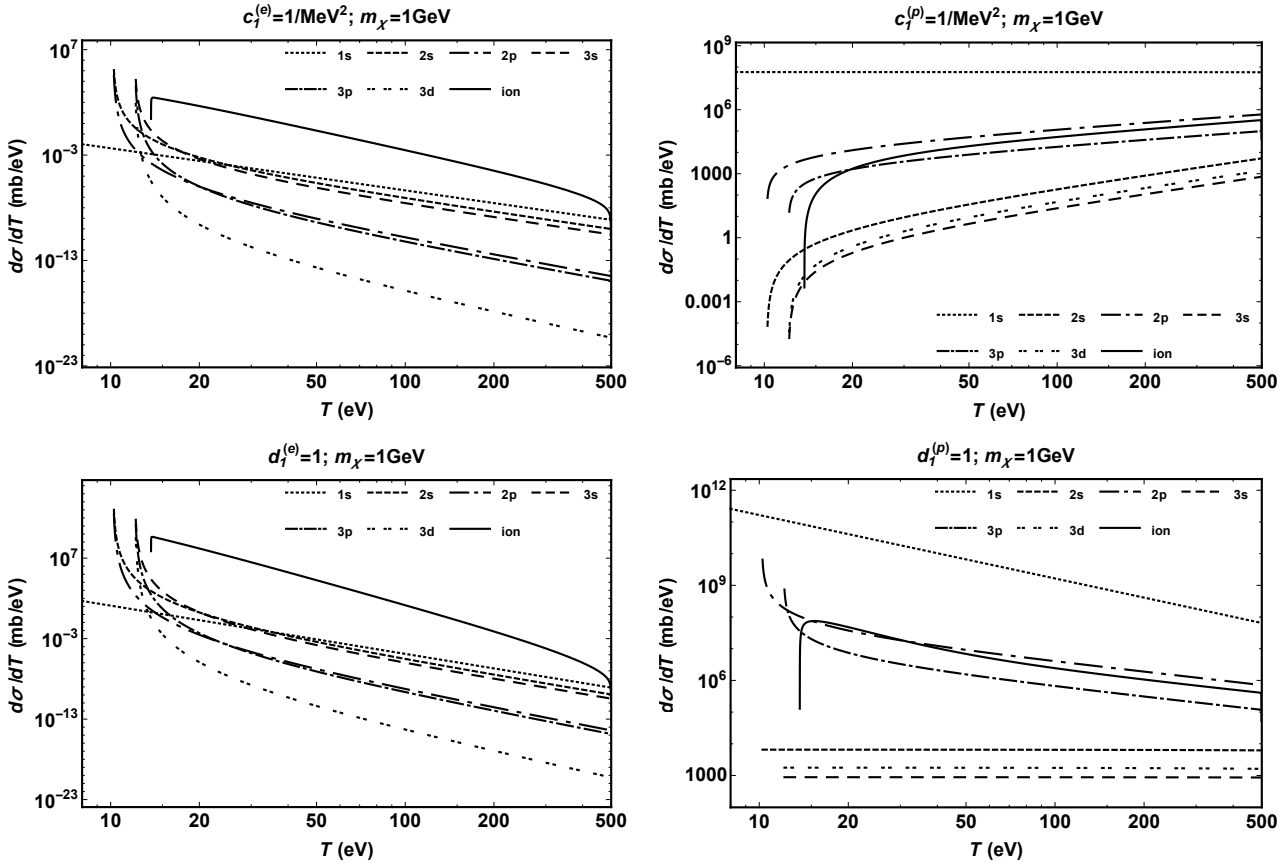

FIG. 1. Different channels of DM scattering with $m_\chi = 1\,\mathrm{GeV}$ and interaction of $c_1^{(e)} = 1/\mathrm{MeV}^2$ (upper-left), $c_1^{(p)} = 1/\mathrm{MeV}^2$ (upper-right), $d_1^{(e)} = 1$ (lower-left), $d_1^{(p)} = 1$ (lower-right).

can be best illustrated by observing the difference of the (almost) flat line and the power-law-decreasing line in the $c_1^{(p)}$ and $d_1^{(p)}$ plots respectively. For discrete excitation channels, except for near-threshold region, one expects similar $1/T^2$ dependence when T gets bigger than excitation energies. The case of ionization channel is more intricate, as q^2 is to be integrated over a range allowed by kinematics; there is no simple scaling from the c_1- to d_1-type results. Overall, the long-range interaction yields sharper energy dependence of $d\sigma/dT$ than the contact one for all scattering channels considered. The elastic scattering is still the best channel to constrain $d_1^{(p)}$, and discrete excitations at thresholds and ionization the best for $d_1^{(e)}$.

In Fig. 2, similar plots but with $m_\chi = 50\,\mathrm{MeV}$ are shown. The most noticeable differences from Fig. 2 are (i) the NR DM kinetic energy is smaller so $T_{\max} = {}^1\!/_2 m_\chi v_\chi^2 = 25\,\mathrm{eV}$ and (ii) in elastic scattering and discrete excitations, the maximum allowed energy transfers are cut off at smaller values: 4.8, 14.0, and 15.7 eV for final $n = 1$, 2, 3, respectively. The latter is

due to maintaining energy and momentum conservation in the final two-body system (the DM particle and the atom) with $m_\chi \leq M_H$. Using Eq. (10) and setting the maximum DM scattering angle $\cos\theta = -1$, one can get an approximate formula

$$T_{\rm cut}^{(nl)} = \frac{4 m_\chi M_H}{(m_\chi + M_H)^2} T_{\rm max} + \frac{M_H - m_\chi}{M_H + m_\chi}(E_{nl} - E_{1s})\,, \tag{24}$$

which yields the correct cut off energies just pointed out. Except the cutoffs in energy transfer, $d\sigma/dT$'s of elastic scattering and discrete excitations are the same for both $m_\chi = 50\,\text{MeV}$ and $m_\chi = 1\,\text{GeV}$ in the allowed range of T. Because the associated response functions, which depend on the 3-momentum transfer q, are fixed by T and excitation energy, the independence of m_χ is thus understood. Note that these cutoff energies limit the ability of direct LDM searches because the recoil energies are too small to be detected.

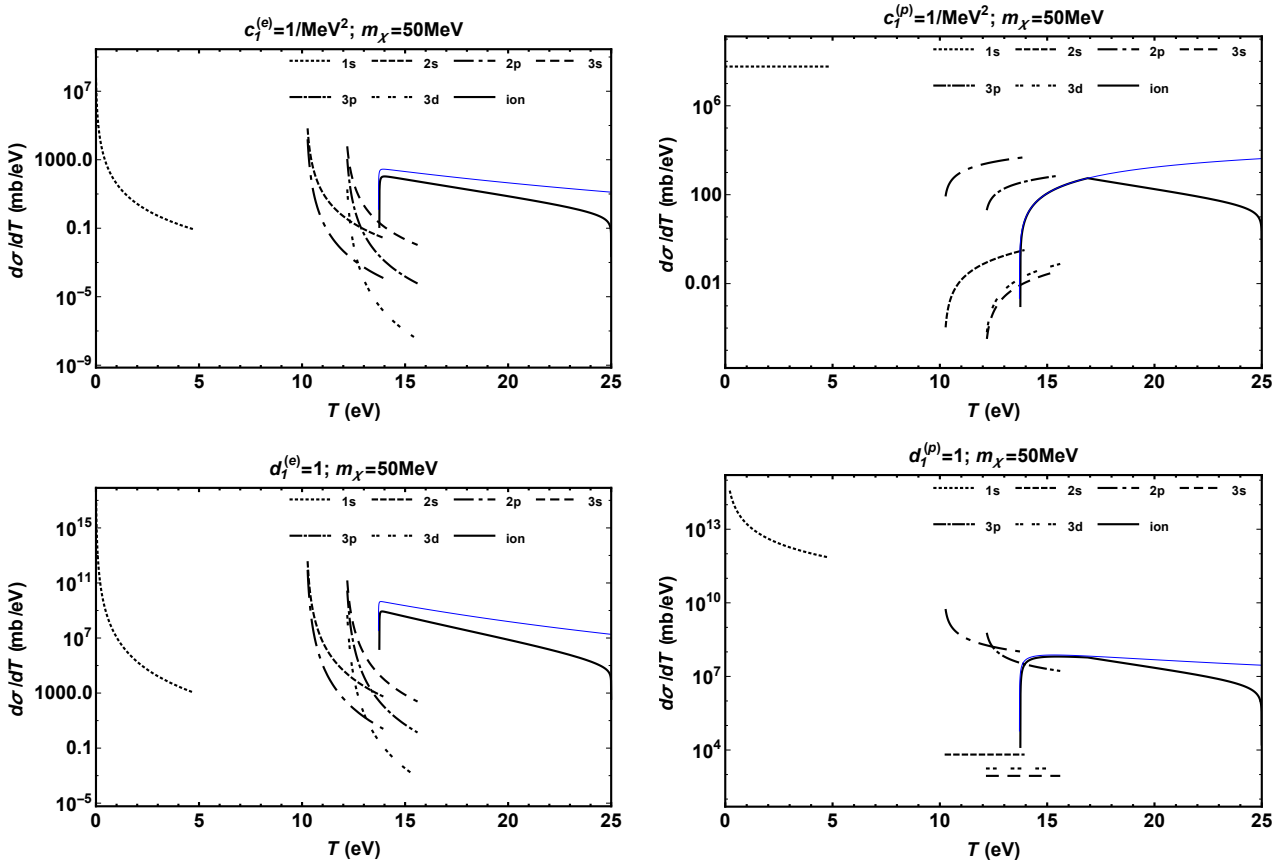

FIG. 2. Different channels of DM scattering with $m_\chi = 50\,\text{MeV}$ and interaction of $c_1^{(e)} = 1/\text{MeV}^2$ (upper-left), $c_1^{(p)} = 1/\text{MeV}^2$ (upper-right), $d_1^{(e)} = 1$ (lower-left), $d_1^{(p)} = 1$ (lower-right). The thin blue curves are the ionization results with $m_\chi = 1\,\text{GeV}$, shown for comparison. (Note. Unlike Fig. 1, these are linear-log plots.)

On the other hand, $d\sigma/dT$ of the ionization channel shows different features. First, as there are three bodies in the final states (the DM particle, the ionized atom, and the ejected electron), energy and momentum conservation does not introduce a kinematic cutoff so T can extend to the end point energy $T_{\rm max}$. For this reason that the ionization channel should be considered as the golden mode to LDM direct searches. Second, the value of q does depend on m_χ, via Eq. (12); as a result, $d\sigma/dT$ is not m_χ independent. To make the comparison clear, the results of $m_\chi = 1\,{\rm GeV}$ are plotted with thin solid curves in the same figures.

At $T \approx 17\,{\rm eV}$, one observes discontinuities in $d\sigma/dT$ on the right panels of Fig. 2. This is a combined result of two ingredients: (i) The scattering angle is bounded by Eq. (12). At $T \approx 17\,{\rm eV}$, the maximum scattering angle 180° is reached (this energy can also be anticipated from Eq. (24) with the excitation energy $E_{nl} - E_{1s}$ being replaced by the binding energy $-E_{1s}$), so the integration range in Eq. (11) ceases to increase for $T > 17\,{\rm eV}$. (ii) The nuclear response function $R_p^{(ion)}$ is bigger at backward angels than forward angels, so the integral Eq. (11) sensitively depends on the integration range and its discontinuity. On the contrary, the electronic response function $R_e^{(ion)}$ is only significant at small angels, therefore the discontinuity in the integration range of Eq. (11) does not yield observable results on the left panels of Fig. 2.

The hydrogen atom only has one electron and one nucleon, so the contributions from the c_4- and d_4-type interactions are related to the ones of the c_1- and d_1-type interactions simply by a rescaling of one-body spin matrix element as discussed in the last section. We shall not repeat these plots, but just note that for other atoms with more electrons and nucleons, the spin-dependent cross sections from interaction terms like c_4 and d_4 do not receive many-body enhancement compared with the spin-independent interactions terms like c_1 and d_1.

As DM interactions with electrons and nucleons are both included in our calculations, it is interesting to compare their contributions. Assuming the same coupling constants, $c_1^{(e)} = c_1^{(p)} = 1/{\rm MeV}^2$, $d_1^{(e)} = d_1^{(p)} = 1$, the comparison shown in Fig. 3 gives several important features:

1. In elastic scattering, the nuclear contribution dominates, and is bigger than the electronic part by several orders of magnitude. Therefore, elastic scattering is not likely to be a good channel of constraining the LO DM-electron interactions, if the LO DM-nucleon interactions are present and not unnaturally suppressed.

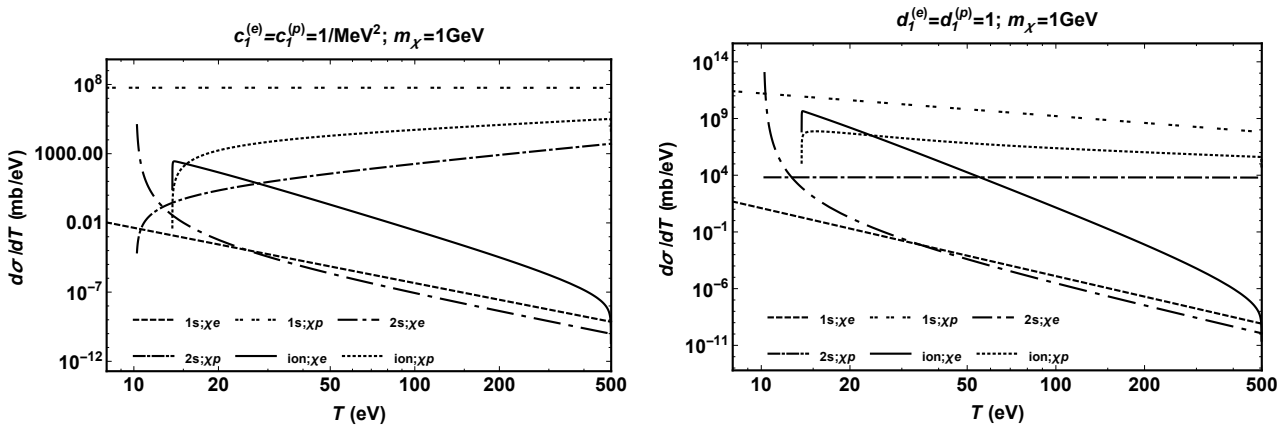

FIG. 3. Comparison of DM cross sections with the electron (χe) and proton (χp) in a hydrogen atom for selected channels including (i) elastic (1s), (ii) discrete excitation to 2s, and (iii) ionization (ion). The interactions are taken to be (Left) $c_1^{(e)} = c_1^{(p)} = 1/\text{MeV}^2$ and (Right) $d_1^{(e)} = d_1^{(p)} = 1$. Interference terms due to χe and χp amplitudes are ignored.

2. In discrete excitations, the nuclear and electronic contributions have sharp crossovers at energies slightly bigger than excitation energies. If a detector is able to resolve these peaks where electronic contributions clearly dominate, then it can be useful for setting more stringent limits on the LO DM-electron interactions.

3. In ionization processes, unlike discrete excitations, the electronic contributions generally dominate over the nuclear parts up to some T beyond the ionization thresholds. As a result, the LO DM-electron interactions can hopefully be constrained in broader kinematic regions.

In Fig. 4, we study the m_χ-dependence of the crossover energy below which the DM-electron cross section begins to be bigger than the DM-proton one (assuming the same coupling strength) via the c_1- or d_1-type interaction that gives rise to hydrogen ionization. The first thing to notice is in both types of interactions and the considered range of m_χ (50 MeV to 5 GeV), there exist certain ranges of DM energy transfer T where the ionization processes are more sensitive to the DM-electron interaction than the DM-nucleon one. Furthermore, one observes that the crossover energy for the d_1-type interaction is larger than the one for the c_1-type interaction. The main reason is the $1/q^4$ factor appearing in the double differential cross section gives more weight to the response function at low q^2, which enhances the role of electrons on one hand and suppresses the role of nucleons on the other.

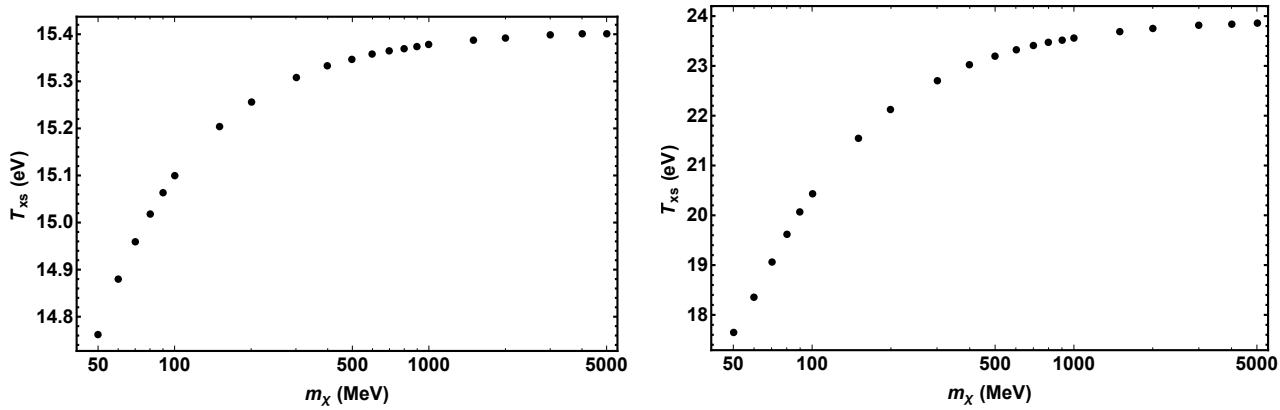

FIG. 4. Energy transfer of DM, $T_{\rm xs}$, below which scattering with electron yield bigger $d\sigma/dT$ than proton in the hydrogen ionization (assuming the same χe and χp coupling strengths), plotted against DM mass m_χ; (Left) for the c_1-type and (Right) for the d_1-type interaction terms.

Therefore, it is reasonable to conclude that the best observational window to look for the LO DM-electron interactions is ionization processes near threshold, in particular for LDM with $m_\chi < M_H$. The discrete excitation peaks (which need good energy resolution of detectors) also provide good supplements. Although hydrogen can hardly be a good candidate for detecting LO DM-electron interactions for the low energy transfer $T \sim 10 - 20\,\text{eV}$ is far below the current detector thresholds, however, our above conclusion makes good sense for practical detector species made of heavy atoms: Not only the ionization thresholds of atomic inner orbitals can be as high as a few or tens of keV which are observable in current detectors, but also there are more than one ionization peaks which can provide additional information.

B. NLO Interactions of c_{11}, d_{11}, c_{10}, and d_{10}

Consider now the interaction terms of c_{11} and d_{11}, the results for $m_\chi = 1\,\text{GeV}$ are presented in Figs. 5. The main change from the corresponding plots of c_1 and d_1 is the extra q^2 factor appearing in the differential cross sections. For elastic scattering or discrete excitations away from threshold, this factor introduces an extra dependence on T, and again can be best seen by a comparison of the $c_1^{(p)}$ and $c_{11}^{(p)}$ curves for elastic scattering. For ionization, the impact of the q^2 factor, which is to be integrated over some allowed range, however can not be easily factored out.

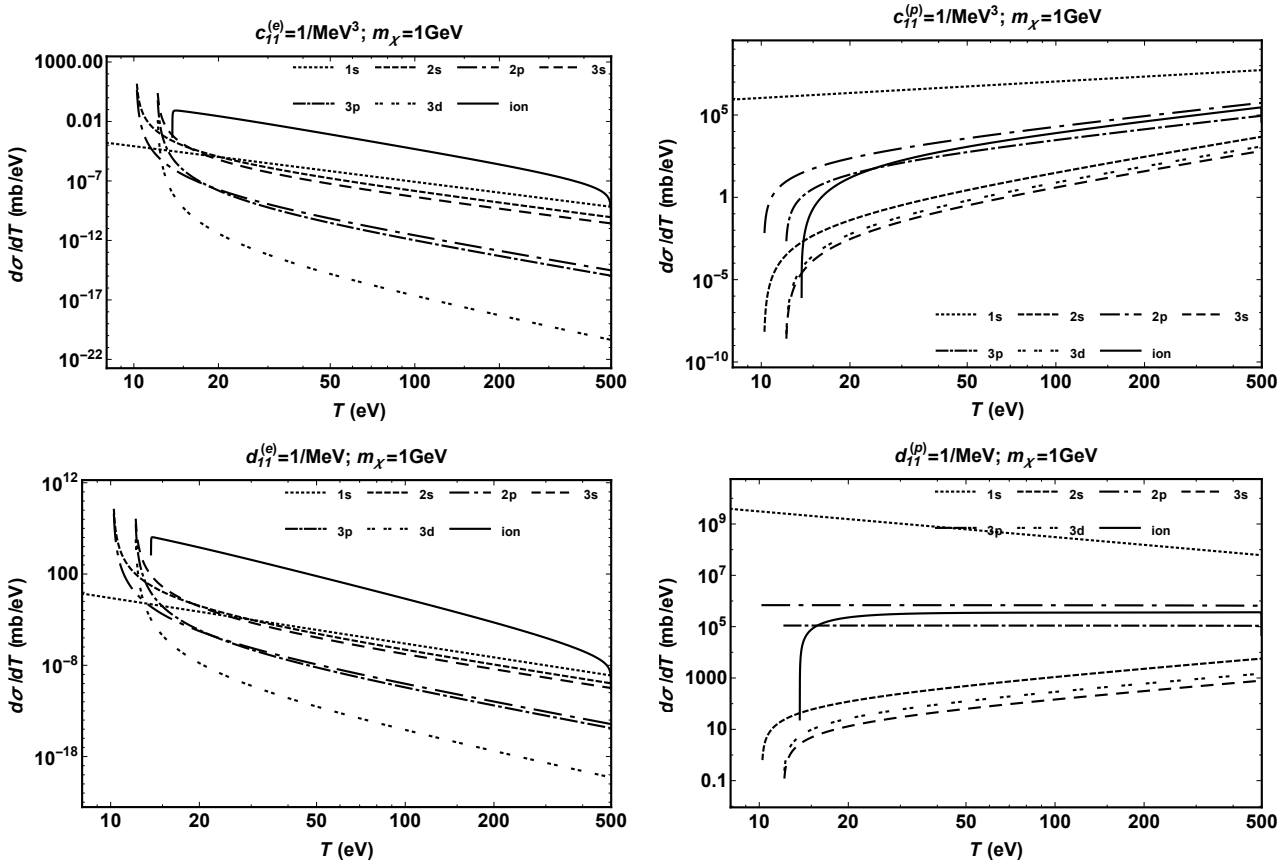

FIG. 5. Different channels of DM scattering with $m_\chi = 1\,\mathrm{GeV}$ and interaction of $c_{11}^{(e)} = 1/\mathrm{MeV}^3$ (upper-left), $c_{11}^{(p)} = 1/\mathrm{MeV}^3$ (upper-right), $d_{11}^{(e)} = 1/\mathrm{MeV}$ (lower-left), $d_{11}^{(p)} = 1/\mathrm{MeV}$ (lower-right).

Our previous argument that $d\sigma/dT$'s of elastic scattering and discrete excitations are independent of m_χ also applies to the cases of c_{11} and d_{11} (also c_{10} and d_{10} to be discussed later). Therefore, we do not repeat the results for $m_\chi = 50\,\mathrm{MeV}$ and just point out that they are the same as for the $m_\chi = 1\,\mathrm{GeV}$ case in the regions bounded by the cutoff energies given by Eq. (24). Also, while the ionization processes do have m_χ dependence, it does not differ from what has been shown in Fig. 2 for the case of c_1 and d_1 in a significant way.

Similarly to the c_1- and d_1-type interactions with DM, elastic scattering is the best to constrain the $c_{11}^{(p)}$ and $d_{11}^{(p)}$ terms, while inelastic scattering at discrete excitation peaks and of ionization are more suitable for the $c_{11}^{(e)}$ and $d_{11}^{(e)}$ terms. To further disentangle the dependence of $d\sigma/dT$ on c_1, d_1, c_{11}, and d_{11}, the scaling of $d\sigma/dT$ with energy transfer T can provide useful guidance: For example, in elastic scattering and discrete excitations away from thresholds, the energy dependence of $d\sigma/dT$ on the $|c_1|^2$, $|d_1|^2$, $|c_{11}|^2$, and $|d_{11}|^2$ terms is T^0, T^{-2}, T^1, and T^{-1}, respectively.

The pattern regarding the competition of electronic and nuclear contributions in discrete excitations and ionization with the c_{11} and d_{11} terms is similar to the case with the c_1 and d_1 terms: sharp crossovers in discrete excitations and some ranges of electronic dominance near ionization threshold. Some examples are given in Fig. 6.

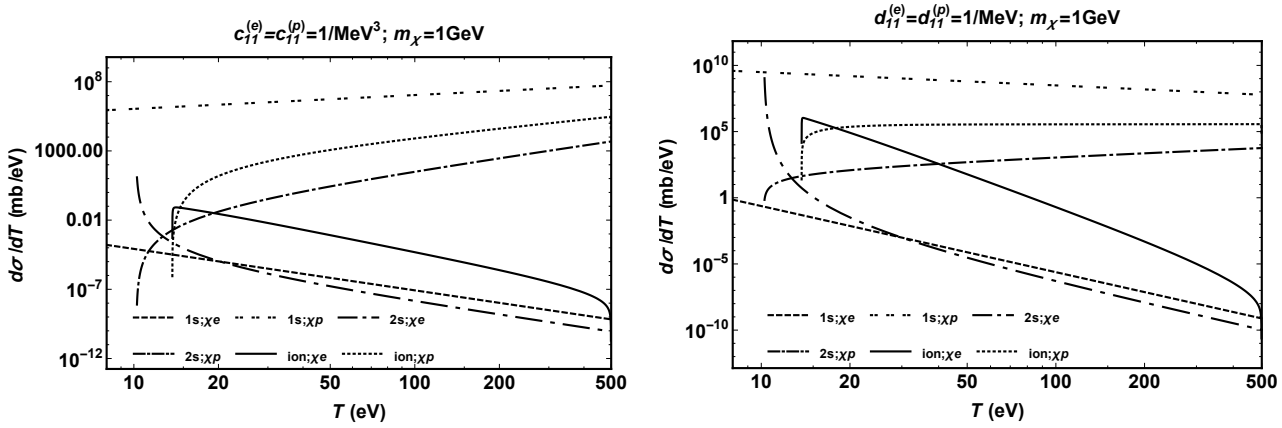

FIG. 6. Comparison of DM cross sections with the electron (χe) and proton (χp) in a hydrogen atom for selected channels including (i) elastic (1s), (ii) discrete excitation to 2s, and (iii) ionization (ion). The interactions are taken to be (Left) $c_{11}^{(e)} = c_{11}^{(p)} = 1/\text{MeV}^3$ and (Right) $d_{11}^{(e)} = d_{11}^{(p)} = 1/\text{MeV}$. Interference terms due to χe and χp amplitudes are ignored.

The energy transfer $T_{\rm xs}$ below which the electronic contribution is bigger than the nuclear one, assuming $c_{11}^{(e)} = c_{11}^{(p)} = 1/\text{MeV}^3$ and $d_{11}^{(e)} = d_{11}^{(p)} = 1/\text{MeV}$, in the ionization processes is plotted in Fig. 7 against m_χ. Notice that the values of $T_{\rm xs}$ for the c_{11}- and d_{11}-type interactions at a given m_χ are both reduced in comparison with the cases of the LO c_1 and d_1 terms, respectively. This is in agreement with the expectation that the extra q^2 factor in the double differential cross section reduces the weight of the small q^2 region, so the electronic contribution is relatively suppressed than the nuclear part.

Similar to the LO case, the contributions from the target-spin-dependent c_{10} and d_{10} terms can be obtained from the target-spin-independent results of c_{11} and d_{11}, simply by adding factors due to spin matrix elements (see Eq. 13). Therefore, all observations and conclusions made in the c_{11} and d_{11} cases apply to the c_{10} and d_{10}.

However, regarding the competition between the electronic and nuclear contributions in scattering processes involving the c_{10} or d_{10} term, there is a subtlety arising from the natural scales of $c_{10}^{(e)}/c_{10}^{(p)}$ and $d_{10}^{(e)}/d_{10}^{(p)}$. If one takes the point of view that both EFT interaction terms of electrons and nucleons are matched to a more fundamental theory at some high scale Λ,

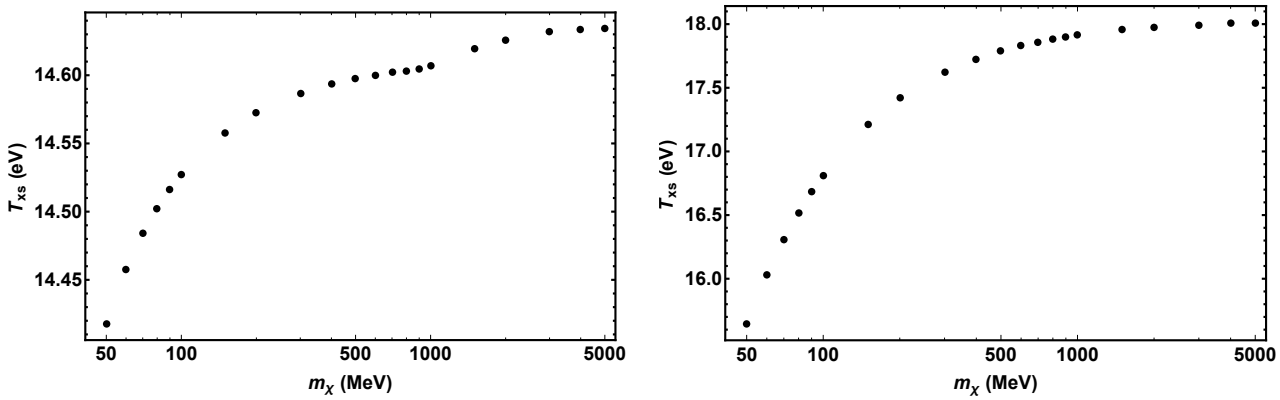

FIG. 7. Energy transfer of DM, $T_{\rm xs}$, below which scattering with electron yield bigger $d\sigma/dT$ than proton in the hydrogen ionization (assuming the same χe and χp coupling strengths), plotted against DM mass m_χ; (Left) for the c_{11}-type and (Right) for the d_{11}-type interaction terms.

then it is reasonable to anticipate the possibility that $c_{10}^{(e)}/c_{10}^{(p)} \sim 1$ and $d_{10}^{(e)}/d_{10}^{(p)} \sim 1$. On the other hand, the masses of an electron and a nucleon differ by three orders of magnitude. If the c_{10} and d_{10} terms are matched to a relativistic theory, for example, $(\bar\chi\chi)(\bar f i\gamma_5 f)$ and $(\bar\chi\chi)(\bar f i\gamma_5 f)/q_\mu^2$ at some high scale, the resulting nonrelativistic EFT expansion at NLO will involve the expansion parameter q/m_f to first order. In such cases, then one should expect $c_{10}^{(e)}/c_{10}^{(p)}$, $d_{10}^{(e)}/d_{10}^{(p)} \sim m_p/m_e \sim 2\times 10^3$. This in turn would largely increase the sensitivity of discrete excitation peaks and ionization processes on the NLO DM-electron interaction terms such as c_{10} and d_{10}.

An example is given in Fig. 8: For $m_\chi \lesssim 160\,\text{MeV}$ and $m_\chi \lesssim 240\,\text{MeV}$ respectively for the c_{10} and d_{10} terms, the electronic contributions are larger than the nuclear ones in the entire allowed ranges of $T \leq {}^1\!/_2 m_\chi v_\chi^2$. For heavier m_χ, the crossovers both happen at energies further away from ionization thresholds, $\sim 50\,\text{eV}$ and $100\,\text{eV}$ respectively for the c_{10} and d_{10} terms – much bigger than other interactions terms previously discussed.

Briefly concluding this subsection, we point out that the best observational window to look for the NLO DM-electron interactions terms including c_{11}, d_{11}, c_{10}, and d_{10} is still the ionization processes near threshold and the discrete excitation peaks. The different energy dependence of $d\sigma/dT$ from the LO terms in principle provides a way to disentangle them. Furthermore, because of the huge difference between the masses of an electron and a nucleon, interaction terms that depend on the relativity of scattered particles can be further separated. In most situations, such NLO DM-electron interactions can be sensitively

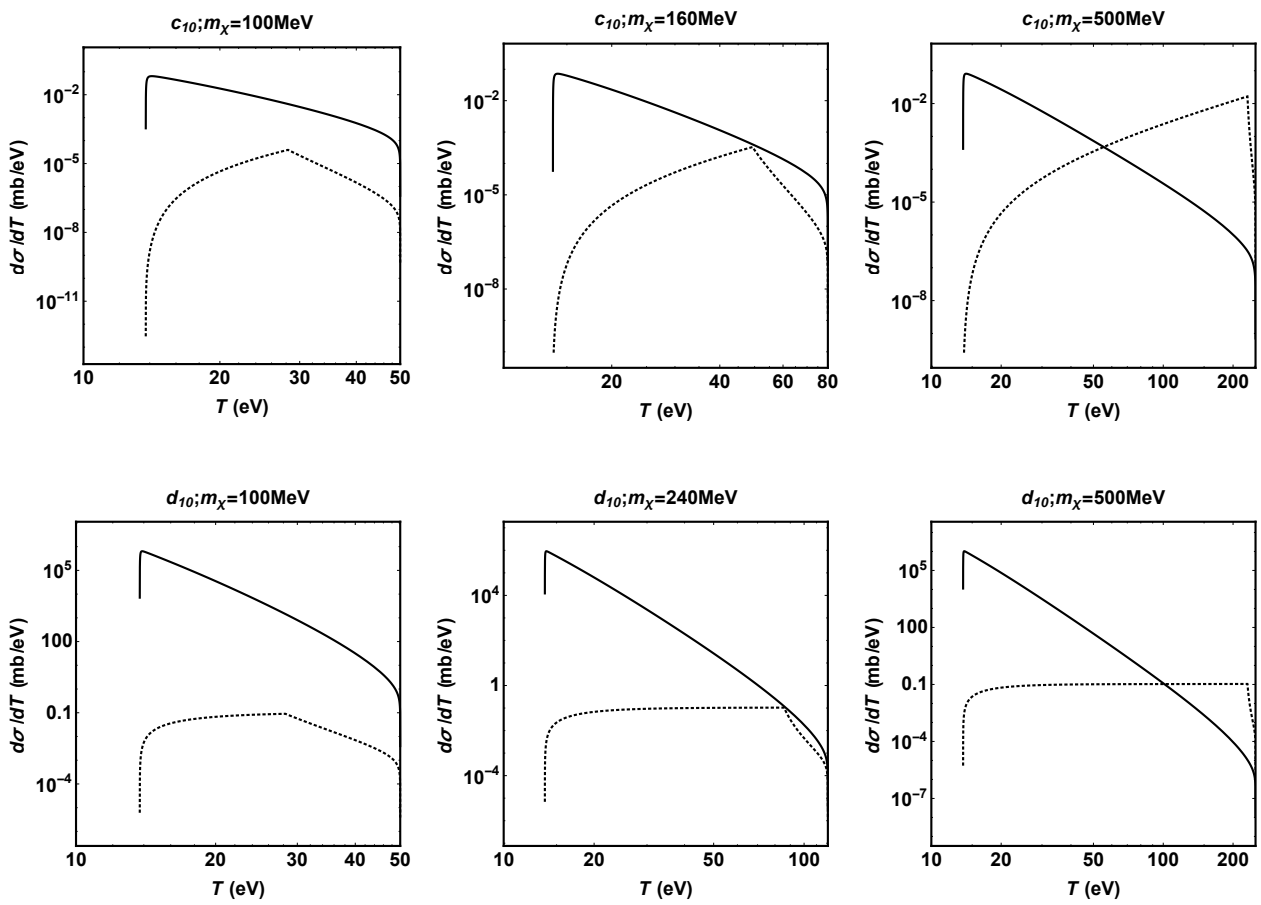

FIG. 8. Comparison of electronic (solid lines) and nuclear (dotted lines) contributions to $d\sigma/dT$ for selected DM mass m_χ with (Upper) $c_{10}^{(e)} = c_{10}^{(p)} m_p^2/m_e^2 = 1/\mathrm{MeV}^3$ and (Lower) $d_{10}^{(e)} = d_{10}^{(p)} m_p^2/m_e^2 = 1/\mathrm{MeV}$.

constrained without much background arising from similar DM-nucleon interactions because atomic electron can be very relativistic while atomic nuclei and nucleons inside are mostly nonrelativistic.

IV. SUMMARY

In this paper, we study the scattering processes of sub-GeV DM particles and hydrogen atoms, including elastic, atomic discrete excitation, and atomic ionization channels. The interactions of DM with electrons and nucleons are both included and formulated in a general framework based on nonrelativistic effective field theory. In addition to the leading-order spin-independent and spin-dependent contact terms, we also include the possibility of long-

ranged DM interactions and a few next-to-leading-order terms. Some of the interaction terms yield orthogonal scattering amplitudes, but there are also interference terms. Disentanglement of various interaction terms can in principle be done by their different dependence on DM energy deposition in scattering cross sections.

On the assumption of same dark matter coupling strengths, it is found that DM–electron interactions dominate the inelastic transitions to discrete excited states and ionization continuum around their threshold regions (sizes of these regions depend on interaction types), and DM–nucleon interactions become more important with increasing energy and dominate in elastic scattering. These conclusions can be used to guide the searches of sub-GeV DM interactions in optimal experimental configurations and kinematics. For DM–electron interactions, the inelastic peaks of discrete excitations and ionizations in scattering cross sections, which can be taken as smoking-gun signals of DM scattering, can further increase an experiment's constraining power. For DM–nucleon interactions, although the elastic scattering is the best channel, however, for light DM particles which can not deposit observable energies in detectors, one has to rely on the high energy part of ionization processes.

The energy and momentum transfers involved in sub-GeV DM scattering overlap typical atomic scales, so studies of issues such as binding effects and electron/nuclear recoil mechanism, which play important roles in interpreting experimental data, require detailed many-body calculations. This case study of hydrogen, where both binding and recoil can be taken into account most simply, therefore provides useful qualitative understanding of what to be anticipated in sub-GeV DM scattering off practical detector materials such as germanium and xenon.

ACKNOWLEDGMENTS

We acknowledge the support from the Ministry of Science and Technology of Republic of China under Grants No. 102-2112-M-002-013-MY3 (J.-W. C., C.-L. W., and C.-P. W.) and No. 103-2112-M-259-003 (H.-C. C. and C.-P. L.); the Center for Theoretical Sciences and Center of Advanced Study in Theoretical Sciences of National Taiwan University (J.-W. C., C.-L. W., and C.-P. W.); and the National Center for Theoretical Sciences. J.-W. C. was also supported in part by the Deutsche Forschungsgemeinschaft and National Natural

Science Foundation of China (CRC 110).

[1] K. Olive *et al.* (Particle Data Group), Chin. Phys. C **38**, 090001 (2014).

[2] R. Essig, J. A. Jaros, W. Wester, P. H. Adrian, S. Andreas, *et al.*, (2013), arXiv:1311.0029 [hep-ph].

[3] J. L. Feng and J. Kumar, Phys. Rev. Lett. **101**, 231301 (2008), arXiv:0803.4196 [hep-ph].

[4] J. L. Feng, M. Kaplinghat, H. Tu, and H.-B. Yu, JCAP **0907**, 004 (2009), arXiv:0905.3039 [hep-ph].

[5] C. Boehm and P. Fayet, Nucl. Phys. **B683**, 219 (2004), arXiv:hep-ph/0305261 [hep-ph].

[6] C. Boehm, P. Fayet, and J. Silk, Phys. Rev. D **69**, 101302 (2004), arXiv:hep-ph/0311143 [hep-ph].

[7] N. Borodatchenkova, D. Choudhury, and M. Drees, Phys. Rev. Lett. **96**, 141802 (2006), arXiv:hep-ph/0510147 [hep-ph].

[8] M. Pospelov, A. Ritz, and M. B. Voloshin, Phys. Lett. B **662**, 53 (2008), arXiv:0711.4866 [hep-ph].

[9] P. Fayet, Phys. Rev. D **75**, 115017 (2007), arXiv:hep-ph/0702176 [HEP-PH].

[10] D. Hooper and K. M. Zurek, Phys. Rev. D **77**, 087302 (2008), arXiv:0801.3686 [hep-ph].

[11] M. Pospelov, A. Ritz, and M. B. Voloshin, Phys. Rev. D **78**, 115012 (2008), arXiv:0807.3279 [hep-ph].

[12] K. Rajagopal, M. S. Turner, and F. Wilczek, Nucl. Phys. B **358**, 447 (1991).

[13] L. Covi, J. E. Kim, and L. Roszkowski, Phys. Rev. Lett. **82**, 4180 (1999), arXiv:hep-ph/9905212 [hep-ph].

[14] K.-Y. Choi, L. Covi, J. E. Kim, and L. Roszkowski, JHEP **04**, 106 (2012), arXiv:1108.2282 [hep-ph].

[15] S. Dodelson and L. M. Widrow, Phys. Rev. Lett. **72**, 17 (1994), arXiv:hep-ph/9303287 [hep-ph].

[16] X.-D. Shi and G. M. Fuller, Phys. Rev. Lett. **82**, 2832 (1999), arXiv:astro-ph/9810076 [astro-ph].

[17] A. D. Dolgov and S. H. Hansen, Astropart. Phys. **16**, 339 (2002), arXiv:hep-ph/0009083 [hep-ph].

[18] A. Boyarsky, J. Lesgourgues, O. Ruchayskiy, and M. Viel, Phys. Rev. Lett. **102**, 201304

(2009), arXiv:0812.3256 [hep-ph].

[19] K. N. Abazajian, Phys.Rev.Lett. **112**, 161303 (2014), arXiv:1403.0954 [astro-ph.CO].

[20] J. Knodlseder *et al.*, Astron. Astrophys. **441**, 513 (2005), arXiv:astro-ph/0506026 [astro-ph].

[21] G. Weidenspointner *et al.*, Nature **451**, 159 (2008).

[22] N. Prantzos *et al.*, Rev. Mod. Phys. **83**, 1001 (2011), arXiv:1009.4620 [astro-ph.HE].

[23] E. Bulbul, M. Markevitch, A. Foster, R. K. Smith, M. Loewenstein, *et al.*, Astrophys. J. **789**, 13 (2014), arXiv:1402.2301 [astro-ph.CO].

[24] A. Boyarsky, O. Ruchayskiy, D. Iakubovskyi, and J. Franse, Phys. Rev. Lett. **113**, 251301 (2014), arXiv:1402.4119 [astro-ph.CO].

[25] D. Hooper and L. Goodenough, Phys. Lett. B , 412 (2011), arXiv:1010.2752 [hep-ph].

[26] D. Hooper and T. Linden, Phys. Rev. D **D84**, 123005 (2011), arXiv:1110.0006 [astro-ph.HE].

[27] R. Essig, J. Mardon, and T. Volansky, Phys. Rev. D **85**, 076007 (2012), arXiv:1108.5383 [hep-ph].

[28] R. Essig, A. Manalaysay, J. Mardon, P. Sorensen, and T. Volansky, Phys. Rev. Lett. **109**, 021301 (2012), arXiv:1206.2644 [astro-ph.CO].

[29] R. Essig, E. Kuflik, S. D. McDermott, T. Volansky, and K. M. Zurek, JHEP **1311**, 193 (2013), arXiv:1309.4091 [hep-ph].

[30] R. Essig, J. Mardon, M. Papucci, T. Volansky, and Y.-M. Zhong, JHEP **11**, 167 (2013), arXiv:1309.5084 [hep-ph].

[31] B. Batell, R. Essig, and Z. Surujon, Phys. Rev. Lett. **113**, 171802 (2014), arXiv:1406.2698 [hep-ph].

[32] R. Bernabei *et al.* (DAMA), Eur. Phys. J. C **56**, 333 (2008), arXiv:0804.2741 [astro-ph].

[33] R. Bernabei *et al.* (DAMA, LIBRA), Eur. Phys. J. C **67**, 39 (2010), arXiv:1002.1028 [astro-ph.GA].

[34] R. Bernabei *et al.*, Eur. Phys. J. C **73**, 2648 (2013), arXiv:1308.5109 [astro-ph.GA].

[35] R. Bernabei, P. Belli, F. Montecchia, F. Nozzoli, F. Cappella, *et al.*, Phys. Rev. D **77**, 023506 (2008), arXiv:0712.0562 [astro-ph].

[36] J. Kopp, V. Niro, T. Schwetz, and J. Zupan, Phys. Rev. D **80**, 083502 (2009), arXiv:0907.3159 [hep-ph].

[37] R. Foot, Phys. Rev. D **90**, 121302 (2014), arXiv:1407.4213 [hep-ph].

[38] O. Adriani *et al.* (PAMELA), Nature **458**, 607 (2009), arXiv:0810.4995 [astro-ph].

[39] O. Adriani *et al.* (PAMELA Collaboration), Phys. Rev. Lett. **111**, 081102 (2013), arXiv:1308.0133 [astro-ph.HE].

[40] M. Ackermann *et al.* (Fermi LAT Collaboration), Phys. Rev. Lett. **108**, 011103 (2012), arXiv:1109.0521 [astro-ph.HE].

[41] L. Accardo *et al.* (AMS Collaboration), Phys. Rev. Lett. **113**, 121101 (2014).

[42] M. Aguilar *et al.* (AMS Collaboration), Phys. Rev. Lett. **113**, 121102 (2014).

[43] J. Fan, M. Reece, and L.-T. Wang, JCAP **1011**, 042 (2010), arXiv:1008.1591 [hep-ph].

[44] A. L. Fitzpatrick, W. Haxton, E. Katz, N. Lubbers, and Y. Xu, JCAP **1302**, 004 (2013), arXiv:1203.3542 [hep-ph].

[45] J.-W. Chen, C.-P. Liu, C.-F. Liu, and C.-L. Wu, Phys. Rev. D **88**, 033006 (2013), arXiv:1307.2857 [hep-ph].

[46] A. Nordsieck, Phys. Rev. **93**, 785 (1954).

[47] A. R. Holt, J. Phys. B **2**, 1209 (1969).

[48] D. Belkić, J. Phys. B **14**, 1907 (1981).

[49] M. S. Gravielle and J. E. Miraglia, Comp. Phys. Comm. **69**, 53 (1992).